Contrasting intrainterstadial climatic evolution between high and middle North Atlantic latitudes: A close-up of Greenland Interstadials 8 and 12

María Fernanda Sánchez Goñi, Amaelle Landais, Isabel Cacho, Josette Duprat, Linda Rossignol

Geochemistry Geophysics Geosystems G3
AN ELECTRONIC JOURNAL OF THE EARTH SCIENCES
Published by AGU and the Geochemical Society

Article
Volume 10, Number 4
28 April 2009
Q04U04, doi:10.1029/2008GC002369
ISSN: 1525-2027

Contrasting intrainterstadial climatic evolution between high and middle North Atlantic latitudes: A close-up of Greenland Interstadials 8 and 12

María Fernanda Sánchez Goñi
EPHE, EPOC, UMR5805, Université Bordeaux 1, CNRS, Avenue des Facultés, F-33405 Talence, France (mf.sanchezgoni@epoc.u-bordeaux1.fr)

Amaelle Landais
Laboratoire des Sciences du Climat et de l'Environnement, UMR1572, IPSL, CEA, CNRS, Bât. 712, Orme des merisiers, F-91191 Gif-sur-Yvette CEDEX, France (amaelle.landais@lsce.ipsl.fr)

Isabel Cacho
GRC Geociències Marines, Departament d'Estratigrafia, Paleontologia i Geociències Marines, Facultat de Geologia, Universitat de Barcelona, C/Martí Franques s/n, E-08028 Barcelona, Spain (icacho@ub.edu)

Josette Duprat and Linda Rossignol
EPHE, EPOC, UMR5805, Université Bordeaux 1, CNRS, Avenue des Facultés, F-33405 Talence, France (jmduprat@orange.fr; l.rossignol@epoc.u-bordeaux1.fr)

[1] Three highly resolved pollen and sea surface temperature records from the Iberian margin (36–42°N) reveal the local evolution of vegetation and climate associated with the rapid climatic variability of marine isotope stage 3. The comparison of the climate at these midlatitudes with δD and d excess from Greenland ice cores shows that the north-south climatic gradient underwent strong variations during the long Greenland Interstadials (GIs) 8 and 12. After the Northern Hemispheric rapid warming at the Greenland Stadial (GS)-GI transition, the trend during the first part of the GI is a Greenland cooling and an Iberian warming. This increase of the North Atlantic climatic gradient led to moisture transportation to Greenland from midlatitudes (lightest d excess) and to a drying episode in Iberia. The subsequent temperature decrease in Greenland and Iberia associated with the precipitation increase in the latter region occurred when the major source of Greenland precipitation shifted to lower latitudes (d excess increase).

Components: 8279 words, 7 figures.

Keywords: Greenland interstadial; Iberia; Dansgaard-Oeschger variability; North Atlantic; precipitation source; pollen.

Index Terms: 0473 Biogeosciences: Paleoclimatology and paleoceanography (3344, 4900); 0426 Biogeosciences: Biosphere/atmosphere interactions (0315); 0428 Biogeosciences: Carbon cycling (4806).

Received 19 December 2008; **Revised** 20 February 2009; **Accepted** 25 February 2009; **Published** 28 April 2009.

Sánchez Goñi, M. F., A. Landais, I. Cacho, J. Duprat, and L. Rossignol (2009), Contrasting intrainterstadial climatic evolution between high and middle North Atlantic latitudes: A close-up of Greenland Interstadials 8 and 12, *Geochem. Geophys. Geosyst.*, *10*, Q04U04, doi:10.1029/2008GC002369.

Theme: Circum-Iberia Paleoceanography and Paleoclimate: What Do We Know?
Guest Editors: F. Abrantes, C. Ruehlemann, M. F. Sánchez Goñi, and A. Voelker

1. Introduction

[2] The millennial climatic variability of the last glacial period (Dansgaard-Oeschger events, hereafter DO events) has been evidenced first by the ice isotopic profile performed on Greenland ice cores [*Dansgaard et al.*, 1984] and then in marine cores of the North Atlantic regions [*Bond et al.*, 1993]. More recently, numerous analyses in continental and marine archives have revealed the large Northern Hemisphere extent of this millennial variability [*Voelker and Workshop Participants*, 2002]. In particular, a number of marine pollen sequences retrieved in the Iberian margin and covering marine isotopic stage (MIS) 3 [*Roucoux et al.*, 2005; *Sánchez Goñi et al.*, 2000, 2002; *Combourieu Nebout et al.*, 2002] have shown the general synchroneity between marine and terrestrial responses in the western Iberian region to the DO climatic variability and, therefore, a dynamic equilibrium between ocean, vegetation and atmosphere during rapid climatic shifts. GSs, defined as intervals of low (ice)/high (sea surface water) $\delta^{18}O$ values during the last climatic cycle, whether associated or not with local iceberg discharges were related to steppe development and cold SST (Sea Surface Temperatures) while GIs, episodes of high (ice)/low (sea surface water) $\delta^{18}O$ values, were contemporaneous with oceanic warming and the expansion of Mediterranean (in the south) and Atlantic (above 40°N) forests.

[3] So far, the Greenland record is often taken as a reference for a Northern Hemisphere climatic variability. Even if the twenty five DO events with the rapid transitions between stadials (generally cold and dry) and interstadials (generally warm and wet) can be identified in different eastern North Atlantic and western Mediterranean marine [e.g., *Shackleton et al.*, 2000; *Sánchez Goñi et al.*, 2008; *Martrat et al.*, 2004] and European [*Genty et al.*, 2003] archives, regional differences should be highlighted. As an example, we have shown that the strongest warming during GIs 19, 12, 11 and 8 in Greenland do not correspond with the maximum expression of the Mediterranean climate (warm, wet winter and dry summer) which occurred during GIs 16–17, 8 and 7 not with the maximum in temperature and moisture in the Atlantic region at DO 14 and 12 [*Sánchez Goñi et al.*, 2008].

[4] Similarly, when scrutinizing the details of the DO events, some strong regional variations have been highlighted. As an example, *von Grafenstein et al.* [1999] have noted a strong contrast during GI 1 (~14.8 ka) between a stable temperature in central Europe and the gradual cooling trend in Greenland revealed by the δD or $\delta^{18}O$ isotopic curves. Similarly, *Genty et al.* [2006] have shown a warming trend during the same period in southern France and northern Tunisia from speleothem analysis. More recently, the interpretation of the combined measurements of δD and $\delta^{18}O$ in the GRIP ice core in term of temperature changes of the evaporative ocean led to a similar conclusion: the relatively low latitude ocean providing water to central Greenland shows a flat temperature evolution during GIs 19, 12, 8 and 1 contrasting with the decrease in Greenland temperature [*Jouzel et al.*, 2007]. Such different behaviors have been interpreted as an increasing cross–North Atlantic climate gradient during GI driven by the east-west and southern migration of the polar front from an East Greenland coastal position.

[5] The previous leading studies have however some limitations. First, *von Grafenstein et al.* [1999] and *Genty et al.* [2006] did local studies only focused on GS 1 during deglaciation which can be affected by many particular processes such as large ice sheets decay and thus a general deglacial reorganization of the European and northern African climates. Second, a temperature change of the evaporative oceanic region reconstructed by water isotopes analyses in ice cores is not necessarily induced by a temperature change of the ocean but can be due to a change in the location of the evaporation region. Thus, the constant surface temperature of the evaporative regions deduced from the water isotopic measurements in the GRIP ice core over GIs is either linked to a constant temperature of the surface ocean at fixed latitude or to a southward shift of the evaporative region associated with a general decrease of the surface ocean temperature. In order to further test the regional contrast during GIs, we focus here on two large GIs associated with DO events 8 and 12 following Heinrich events (H) 4 and 5, respectively

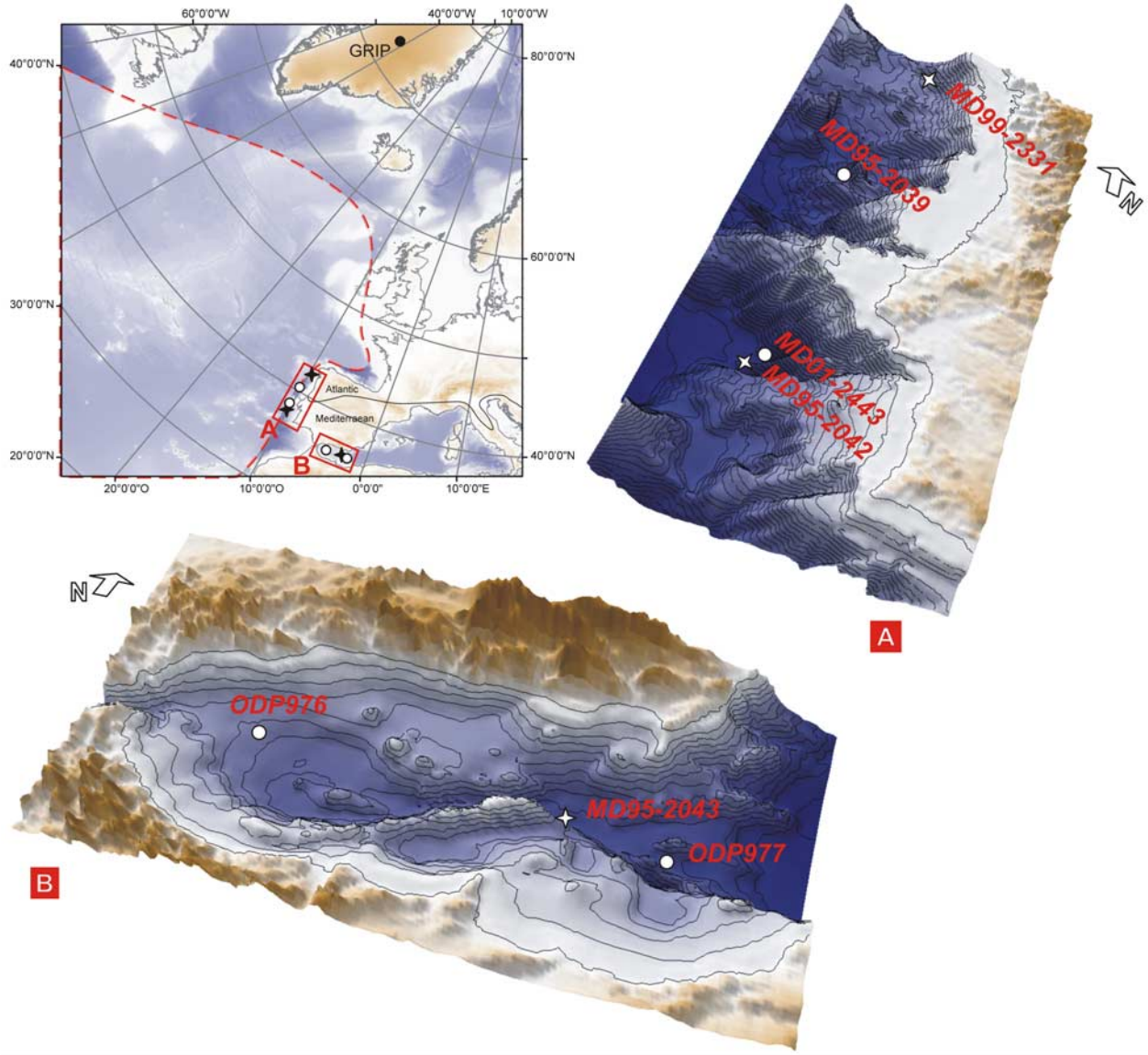

Figure 1. Location of the GRIP ice core and the marine sequences discussed in the text. Black line indicates the limit between the Mediterranean and Atlantic climatic regions [*Polunin and Walters*, 1985]. Dashed red line delimiting a light blue surface between roughly 15°N and 55°N indicates the present-day main evaporative sources of precipitations in central Greenland [*Werner et al.*, 2001].

during MIS 3, i.e., during a period of relatively small changes in ice sheet size. We will therefore present two new and highly resolved palaeoclimatic records, MD95-2042 and MD99-2331, of temperature and precipitation in the southwestern European margin and the adjacent borderlands. These records along with the one already published from the Alboran Sea (core MD95-2043) [*Sánchez Goñi et al.*, 2002] will be compared with the Greenland temperature record inferred from the GRIP δD record and oceanic source temperature inferred from the GRIP δ^{18}O and δD records. This comparison will allow us to discuss the mechanisms underlying the contrasting climatic trends observed between Greenland and the midlatitudes of the eastern North Atlantic and western Europe following Greenland warming events.

2. Present-Day Environmental Setting

2.1. Climate and Vegetation

[6] The spatial pattern of the mean annual precipitation on Greenland has been simulated by the AGCM ECHAM-4 model [*Werner et al.*, 2001]. The simulation shows that the main precipitation

sources for Greenlandic coastal regions are the surrounding polar seas (annual mean SST $\leq$ 10°C) while the midlatitudinal and subtropical Atlantic regions (annual mean sea surface temperatures, SST, between 10°C and 25°C) and the North American continent are the two major source regions of water to central Greenland (Figure 1). The main transport direction from North Atlantic water masses is from the east and can be related to the Iceland low [*Werner et al.*, 2001].

[7] Iberia is the westernmost European peninsula and is characterized at present by two distinct biogeographical regions: the Mediterranean (~40–36°N) and the Atlantic (~40–42°N) regions (Figure 1). The climate of both regions is strongly influenced in winter by the North Atlantic Oscillation (NAO) which is defined as the pressure gradient between the Icelandic Low and the Azores High. Strong gradients, positive mode of the NAO, determine winter dryness in Iberia and high rainfall levels in northern Europe while weak gradients produce the southward displacement of the westerlies bringing moisture to Iberia at expenses of lowering precipitations in northern European latitudes [*Hurrell*, 1995; *Trigo et al.*, 2004]. In summer, in contrast, strong anticyclonic cells develop over the subtropical eastern Atlantic Ocean, producing the characteristic dry season in the western Mediterranean region [*Rodwell and Hoskins*, 2001].

[8] At latitudes above 40°N, these atmospheric configurations result in a wet climate throughout the year, with annual precipitations (Pann) ~1000 mm, and a mean annual temperature of 10°C allowing the development of the Atlantic forest [*Ozenda*, 1982] mainly composed at low elevations of deciduous *Quercus* (oak). In the Mediterranean region, precipitation is concentrated in autumn and winter. Cool winters (minimal winter temperatures ranging between 5 and −1°C) and hot, dry summers (Pann < 600 mm) promote the development of Mediterranean forest made up of *Pinus*, evergreen and deciduous *Quercus* along with thermophilous elements (*Olea*, *Phillyrea*, *Pistacia* and *Cistus*) in the lowlands [*Blanco Castro et al.*, 1997].

2.2. Oceanography and Sedimentation Processes in the Iberian Margin

[9] The hydrological structures and currents as well as the sedimentary processes of the western Iberian margin, from which cores MD95-2042 and MD99-2331 have been collected, are thoroughly described by *Naughton et al.* [2007]. This region is dominated at the surface by the southern branch of the North Atlantic Drift. Sediment supply, including pollen grains, is mostly derived from the Douro and Miño-Sil rivers in the north, and from the Tagus river through canyons and by offshore filaments in the south. The detailed comparison of modern pollen spectra from the uppermost sediments of the Ria de Vigo (mouth of the Miño river) and that of the top of core MD99-2331 shows that their pollen content is similar. The same similarity is observed between the modern pollen sample from the locality of Barreiro (Tagus estuary) and those from the top of core MD95-2042 [*Naughton et al.*, 2007]. Experimental studies have shown [e.g., *Peck*, 1973; *Heusser and Balsam*, 1977; *Heusser*, 1985] the primary importance of the fluviomarine sedimentation of pollen grains in the marine realm. Therefore, pollen grains in the sediments of deep-sea cores MD99-2231 and MD95-2042 were most likely recruited by the streams of the Miño-Sil and Douro basins and the Tagus river from the vegetation colonizing the related hydrographic basins, respectively [*Naughton et al.*, 2007]. Airborne pollen input was certainly of minor importance because of the predominant North Atlantic westerly wind direction in this region.

[10] In the Alboran Sea, the westernmost part of the Mediterranean basin, the less dense Atlantic water crosses the Strait of Gibraltar forming the upper layer which flows toward the eastern Mediterranean Sea [*La Violette*, 1986]. Sedimentary supply close to the site of core MD95-2043 indicates that the main proportion of lithogenic particles reaching this site is related with the strong riverine input which characterizes the torrential rain regime in southeastern Spain [*Fabrès et al.*, 2002]. Other studies show clear evidence for an association between sedimentation of pollen and fine mineral particles in marine depositional environments [*Peck*, 1973]. We consider, therefore, that the main source area of the pollen preserved in core MD95-2043 is southeastern Iberia. However, the continuous record of *Cedrus*, a native tree of the Atlas mountain chain, indicates that some amount of pollen from northern Africa is also incorporated in the sediments of the Alboran Sea potentially by aeolian transport as the present-day sedimentation at the site of core MD95-2043 is dominated by river input from the north.

3. Material and Methods

3.1. Marine Cores

[11] Cores MD95-2042, MD95-2043 and MD99-2331 have been extensively studied for the interval

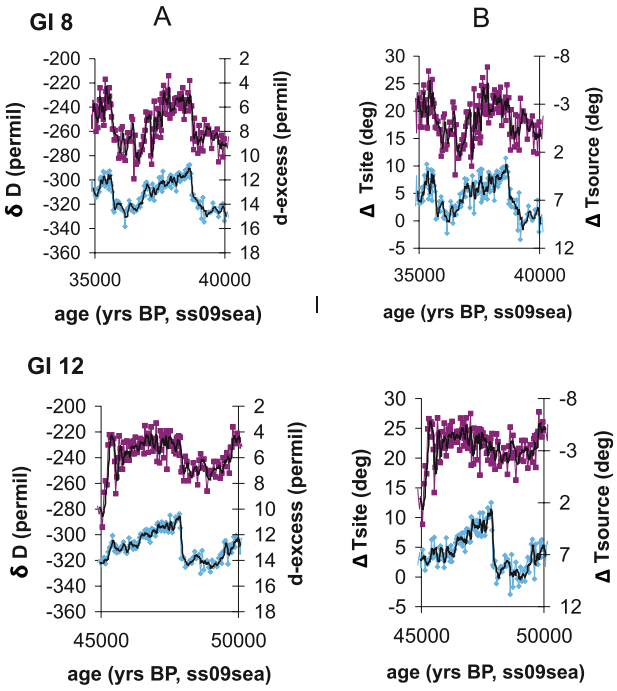

Figure 2. (a) Record of δD (blue) and d excess (magenta) over GIs 8 and 12 from the GRIP ice core [*Dansgaard et al.*, 1993; *Masson-Delmotte et al.*, 2005; *Jouzel et al.*, 2007]. Both proxies are expressed in V-SMOW. (b) Reconstruction of relative variations in T_{site} (ΔT_{site}, blue) and relative variations in T_{source} ($\Delta_{Tsource}$, magenta) over GIs 8 and 12 from the δD and d excess data displayed in Figure 2a. Moving averages (5 points) are displayed in black.

50–27 ka (thousands of years before present) [e.g., *Shackleton et al.*, 2000; *Sánchez Goñi et al.*, 2000], the last 50 ka [*Cacho et al.*, 1999; *Fletcher and Sanchez Goñi*, 2008], and the last 25 ka [*Naughton et al.*, 2007], respectively. These studies based on ice rafted debris counts, isotopic and magnetic measurements and foraminifer and alkenone-derived analyses reveal the impact of H events and DO events in the SST and vegetation evolution over northwestern and southern Iberia according to the analysis of pollen grains from the same sample set. So far, however, the precise evolution of the vegetation and climate of these regions within a GI has not been discussed in detail partly because of the lack of enough resolution in previous studies. We present here, for the first time, the detailed succession of vegetation and terrestrial climate of the north and southwestern regions over MIS 3 (60–27 ka), including a higher resolution of the published interval of MD95-2042 (50–27 ka), along with the record of winter and summer SST from the analysis of foraminifer assemblages of the latter core.

[12] Eighty eight and eighty five samples were analyzed for pollen in the interval encompassing MIS 3 in cores MD95-2042 and MD99-2331, respectively. The resolution of the analysis varies between 2 cm and 12 cm, with the highest resolution for the sections corresponding to GIs 12 and GI 8 (100 to 400 years). The preparation technique follows the protocol established at the UMR EPOC, Bordeaux 1 University (http://www.epoc.u-bordeaux.fr/) and is similar to that used in our previous works.

[13] The analysis of foraminifer assemblages was performed with slightly higher resolution than that applied for the pollen counting. February and August SST values were estimated applying the Modern Analogue Technique (MAT) transfer function from the database of *Pflaumann et al.* [1996] improved during the MARGO project [*Kucera et al.*, 2005] to the planktic foraminifer assemblages. This MAT uses a database including 862 present-day foraminifer assemblages distributed over the North Atlantic Ocean. For cores MD95-2042 and MD99-2331, the average estimation error for February and August SST is ±1.2°C and ±1.5°C, respectively.

3.2. GRIP Isotopic Curves

[14] The Greenland GRIP ice core has been retrieved in 1992 at Summit. δ^{18}O measurements were then performed on 55 cm length samples in 1993 [*Dansgaard et al.*, 1993] and the corresponding profile of δD obtained in 1995 [*Masson-Delmotte et al.*, 2005; *Jouzel et al.*, 2007]. It has been shown that although δD or δ^{18}O records indicate the past temperature variations, no quantitative estimates of temperature can be obtained from these records in Greenland especially for the last glacial period [*Jouzel*, 1999]. The d excess is a second-order parameter defined as d excess = δD − 8 * δ^{18}O [*Dansgaard*, 1964]. Simple isotopic models [e.g., *Johnsen et al.*, 1989; *Ciais and Jouzel*, 1994] have suggested a strong link between d excess and the temperature of the evaporative ocean, hereafter T_{source}. Superimposed to the dependency of δD on local temperature, hereafter T_{site}, and of d excess on T_{source}, these models have shown that δD is also influenced by T_{source} and d excess influenced by T_{site}. However, combining δD and d excess measurements with simple isotopic models enables one to decipher the T_{site} and T_{source} evolutions [e.g., *Vimeux et al.*, 2001; *Stenni et al.*, 2001].

[15] In order to retrieve a record of T_{site} and T_{source} for GI 8 and 12 from the combined measurements

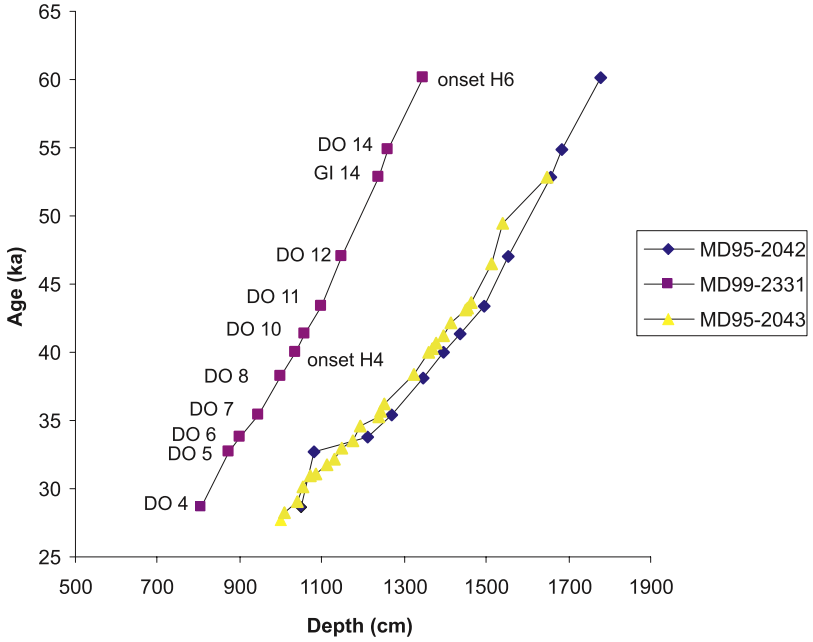

Figure 3. Age versus depth model for the three cores discussed in this study.

of δD and d excess (Figure 2a), we followed the same method as described by *Masson-Delmotte et al.* [2005]. We deduced quantitative and δD-independent estimates of T_{site} changes over the transition between GSs and GISs with a method based on $\delta^{15}N$ and $\delta^{40}Ar$ measurements in the air trapped in ice cores, (*Landais et al.* [2004] for GI 12 and *Severinghaus et al.* [2003] for GI 8). Then, we used an isotopic model of Rayleigh distillation [*Ciais and Jouzel*, 1994] tuned for the GRIP site [*Masson-Delmotte et al.*, 2005] to quantify the influence of T_{site} and T_{source} on δD and d excess. After inversion, we obtained reconstruction of T_{site} and T_{source} as depicted in Figure 2b. Comparisons of T_{site} and T_{source} reconstructions with δD and d excess show that the general evolution inferred from δD and d excess during GSs and GIs remains unchanged while the transition between a GS and a GI is more marked in T_{site} than in δD and less marked in T_{source} than in d excess. Thus, in the following, we confidently interpreted the δD and d excess changes over the DO events of MIS 3 in term of changes in T_{site} and T_{source}, respectively.

[16] Note that temperature reconstruction from ice proxies are derived from both water and air isotopes. The use of air isotopes permits to quantify the local temperature changes and does not depend of sources of water, seasonality of precipitation, altitude nor sea level changes. Moreover, combining δD and d excess permits the removal of the trend due to changes in the source of water in the evolution of the site temperature deduced from δD. Finally, when comparing site temperature reconstructed by air isotopes on the one side and by a combination of δD and d excess on the other side over a DO event, an excellent agreement is obtained [*Landais et al.*, 2004] so that we believe that the site temperature reconstructions presented in this paper are rather robust.

3.3. Chronology

[17] The age model of the western Iberian marine cores MD95-2042 and MD99-2331 is based on a number of calibrated radiocarbon dates and the stratigraphical correlation of warming episodes in marine and terrestrial environments with DO events [*Sánchez Goñi et al.*, 2008] (Figure 3). The chronology of core MD95-2043 is derived from that of *Cacho et al.* [1999]. However, it has been slightly modified for the interval 50–40 ka which now is aligned to the western Iberian margin cores. Moreover, the layers identifying the H events in these cores are strong stratigraphical markers permitting the establishment of a reliable correlation between sites. One additional marker derives from the identification in the two western Iberian margin cores of a change in the coiling ratio of *Globigerina hirsuta* from the left to the right within GI 14 (52.8 ka). The chronology of GRIP excess and deuterium records derives from the revised GRIP time scale (SS09sea) of *Johnsen et al.* [2001]. The ice and marine chronologies differ by around 500 years in average in the intervals encompassing GIs 12 to 9 and GIs

8 to 5. This mismatch is likely the result of the different chronologies, GISP2 and SS09sea, applied to marine and ice archives, respectively, on the interval 47–31 ka.

4. New Results From Pollen Analysis

[18] Figures 4a and 4b display the detailed pollen percentage diagrams of the MIS 3 interval with selected taxa from cores MD95-2042 and MD99-2331. Additionally, we have calculated pollen concentrations for these western Iberian margin cores and drawn the curves in Figures 4a and 4b. The pollen concentration profile from core MD95-2043 (Alboran Sea) was published by *Sánchez Goñi et al.* [2002]. The comparison between these pollen concentration profiles and the respective pollen percentage curves of Mediterranean and Atlantic forests shows that there is no parallelism between them. This indicates that the observed trends in the percentage curves and, therefore, in the derived climate changes are independent from pollen input variations.

[19] In order to facilitate the interpretation of the pollen percentage diagrams, we have established a pollen zonation following the definition by *Birks and Birks* [1980]. A pollen zone is defined as a body of sediment with a consistent and homogeneous fossil pollen content which is different from that preserved in the adjacent sediment bodies. In general, a pollen zone includes more than one pollen sample but certain zones of our diagrams have been established on the basis of a single sample. Increasing the sampling resolution of these particular intervals should confirm the identification of these one sample-based pollen zones.

[20] In the MD95-2042 pollen diagram, twenty seven pollen zones have been identified which for the interval between 48 ka and 28 ka are almost the same as those published in *Sánchez Goñi et al.* [2000]. Uneven pollen zones MD42-3-1 to MD42-3-23 are characterized by relatively high percentages of deciduous *Quercus*, *Betula*, Mediterranean trees (evergreen *Quercus* and *Olea*) and shrubs (*Pistacia*, *Cistus* and *Phillyrea*) along with the increase of Ericaceae (heather). These zones reveal Mediterranean forest expansions and, therefore, interstadial periods, i.e., warm and dry summers but humid winters. In contrast, even pollen zones MD42-3-2 to MD42-3-26 identify episodes of semidesert expansion dominated by *Artemisia*, Chenopodiaceae and *Ephedra*, taxa defining the Mediterranean steppe and, therefore, cold and winter dry climate in southwestern Iberia during stadial periods. In this region, transitions from stadial to interstadial periods of the last glacial are defined by increases of ~5 to 30% in Mediterranean forest pollen content. Zones MD42-3-25 and 27, marked by the development of heathlands at expenses of semidesert formations, are also considered as interstadial periods though the Mediterranean forest cover remains reduced. Ericaceae needs at least 4 months of mean temperatures above 10°C while the forest in temperate latitudes requires a longer period of warmth with a growth period of 4–6 months, and cool but mild winter of 3–4 months [*Polunin and Walters*, 1985]. These zones approaching the last glacial maximum indicate episodes of substantial increase of moisture but weaker warming than those of previous interstadials. Direct correlation of uneven pollen zones with marine proxies (Figure 5) confirms that they correspond to GIs 17 to 3. Interestingly, GIs 17–16 and 8 reveal intervals with the maximum development of Mediterranean trees and shrubs but relatively weak development of Ericaceae in comparison with that observed during GIs 14 and 12. Because Ericaceae species require high atmospheric humidity [*Polunin and Walters*, 1985], GIs 17–16 and 8 indicate the maximum expression of the Mediterranean climate at those times with annually less rainfall than GIs 14 and 12.

[21] The pollen record from MD95-2043 reveals a similar pattern than that of core MD95-2042, confirming that the climate during GI 8 had a more Mediterranean character than that of GI 12 and 14. However, the respective semidesert and Mediterranean forest formations were more developed in the southeastern part of Iberia than in the southwestern part of this peninsula and, a minor proportion of Ericaceae colonized the borderlands of the Alboran Sea during MIS 3. An east-west precipitation gradient, similar to that of the present day, occurred in Iberia independently of the ice sheet size [*Sánchez Goñi et al.*, 2002].

[22] The pollen analysis of the northern Iberian core MD99-2331 reveals an alternation between steppe-dominant vegetation (*Calluna*, Ericaceae, Poaceae, *Taraxacum*-type and *Helianthemum*) and Atlantic forest expansion (mainly deciduous *Quercus* and *Betula*) with *Pinus* development. Uneven pollen zones MD31-3-1 to 23 reveal interstadial periods the warmest of which are represented by zones MD31-3-5 and MD31-3-9. Even pollen zones MD31-3-2 to MD31-3-22 detect stadial periods. In northwestern Iberia, the stadial-interstadial transitions are

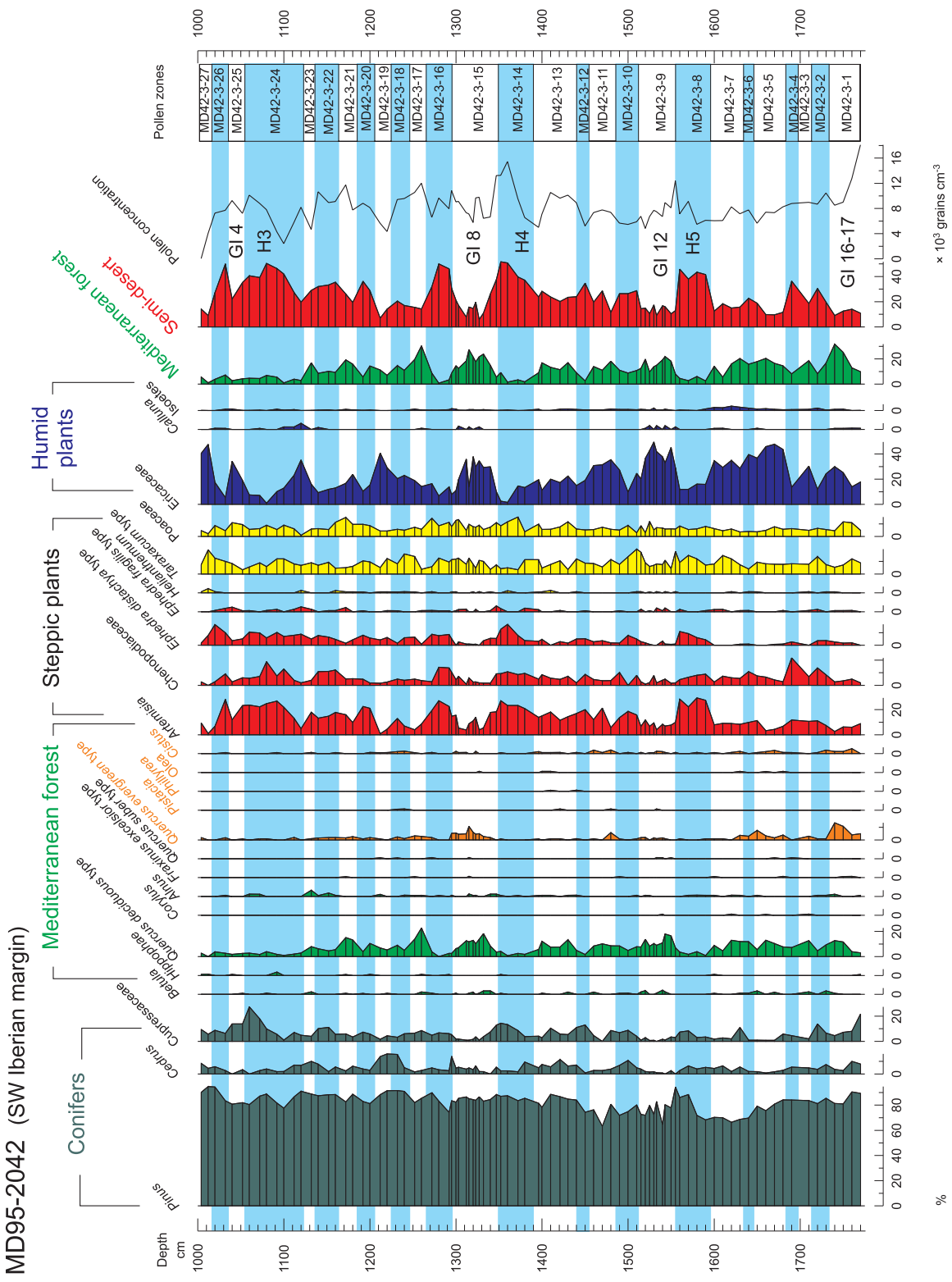

Figure 4a. Pollen percentage diagram with selected taxa for the section of core MD95-2042 corresponding to MIS 3 and total pollen concentration curve.

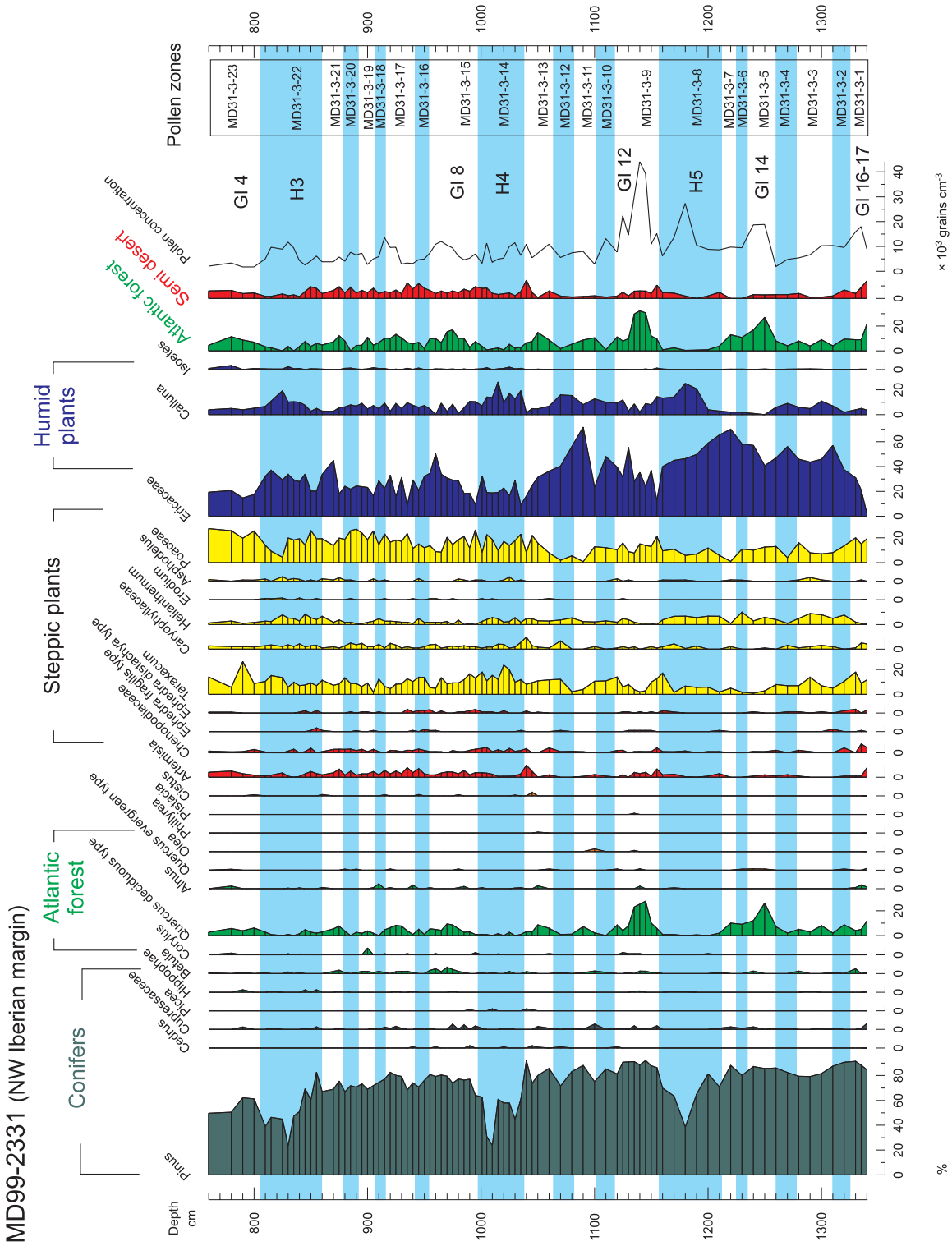

Figure 4b. Pollen percentage diagram with selected taxa for the section of core MD99-2331 corresponding to MIS 3 and total pollen concentration curve.

marked by increases of 5 to 30% in the Atlantic forest pollen percentages. The comparison between pollen and marine proxies (Figure 5) shows that excluding GI 15 which is not clearly expressed in the Atlantic pollen record, these repeated expansions of the Atlantic forest correspond with GIs 17 to GI 3. The warmest interstadials, MD31-3-5 and MD31-3-9, coincide with GIs 14 and 12. Among the stadial periods, zones MD31-3-6, MD31-3-12 and MD31-3-22 are characterized by the highest percentages of *Calluna* indicating the coldest and wettest stadials in northwestern Iberia as this genus colonizes the mires of the present-day Boreal vegetation located above 60°N [*Polunin and Walters*, 1985]. These coldest periods on land are contemporaneous with the H 5, 4 and 3.

5. Discussion

5.1. Land-Sea Correlation Along the Iberian Margin and Relation to Greenland MIS 3 Variability

[23] Figure 5 shows the direct correlation between marine and terrestrial climatic indicators from the three Iberian margin cores compared with δD and d excess records. The Greenlandic δD (T_{site}) curve permits identifying the succession of GIs and GSs on the sequence of DO events. It shows that the GS-GI transition involved rapid (in less than 100 years) and abrupt (8–16°C) increases of T_{site} [*Huber et al.*, 2006; *Masson-Delmotte et al.*, 2005] followed by an stepwise cooling trend for all the GIs.

[24] At lower latitudes, GIs were associated with the development of forest and expansion of heathlands in Iberia thus characterizing warm and wet episodes. They also correspond to relatively high SST in the Iberian margin (~20°C in summer and 12°C in winter in the south; 16°C in summer and 10°C in winter in the north). In contrast, the d excess (T_{source}) record shows lower values during GIs thus suggesting either colder oceanic temperature at midlatitudes or a northern migration of the evaporative region. Since, colder SST at intermediate latitudes during GIs are not supported by our marine data and other records from North Atlantic midlatitudes [*Sachs and Lehman*, 1999; *Vautravers et al.*, 2004], we better associate the lower d excess values to a northward shift of the evaporative source [*Masson-Delmotte et al.*, 2005]. GSs are in turn synchronous with steppe development, hence cold and dry conditions, in Iberia and cold SST offshore. On the basis of the same argumentation as above, we attribute the high values of d excess observed during GSs to a southern source of moisture for Greenland during the GSs as compared to GIs.

[25] Notable differences can be observed in the amplitude of the vegetation changes associated with the DO climatic variability in the different records. The Mediterranean locations show maximum values, higher than 20%, in forest development during GIs 7, 8 and 16–17 coinciding with minima in precession while the maximum development, amplitude changes higher than 20%, of the Atlantic forest (above 40°N) occurred during GIs 12 and 14 when obliquity is at a maximum. This different character of the GIs is not detected in the Greenlandic δD record in term of the amplitude of individual GIs. All the long GIs recorded in Greenland (GIs 17–16, 14, 12, and 8) are associated with significant vegetation signals in the low-latitude marine cores, but the response is very variable according to the region. Additionally, some of the most prominent vegetation signals are not necessarily associated with a long-lasting GI (i.e., GI 7). These observations indicate that orbital parameters modulate the impact of the glacial DO events and provide a strong regional character to this global climate variability [*Sánchez Goñi et al.*, 2008].

5.2. Intrainterstadial Climatic Evolution During GIs 8 and 12

[26] In order to analyze in detail the climatic evolution within a GI, we have chosen two long

Figure 5. Ice, terrestrial and marine proxy records of MIS 3. Core MD99-2331: (a) Pollen percentages of the Atlantic forest, mainly deciduous *Quercus* and *Betula* (green line), (b) pollen percentages of *Calluna* (light blue line), and (c) winter and summer SSTs from the analysis of foraminifer assemblages. Core MD95-2043: (d) Pollen percentages of Mediterranean trees and shrubs (evergreen *Quercus*, *Olea*, *Pistacia*, *Phillyrea*, and *Cistus*) (orange line) and pollen percentages of the Mediterranean forest (mainly deciduous *Quercus* plus Mediterranean trees and shrubs) (green line) and (e) $U^{k}_{37'}$-derived SST [*Cacho et al.*, 1999]. Core MD95-2042: (f) Pollen percentages of Mediterranean trees and shrubs (evergreen *Quercus*, *Olea*, *Pistacia*, *Phillyrea*, and *Cistus*) (orange line) and pollen percentages of the Mediterranean forest (mainly deciduous *Quercus* plus Mediterranean trees and shrubs) (green line), (g) pollen percentages of semidesert plants (*Artemisia*, *Chenopodiaceae*, and *Ephedra*) (red line) and pollen percentages of Ericaceae (blue line), (h) winter and summer SSTs from the analysis of foraminifer assemblages, and (i) IRD concentrations. GRIP ice core: (j) d excess curve and (k) deuterium curve. Both proxies are expressed in V-SMOW. Arrows indicate the highest SST values in the middle of GIs 8 and 12 in the Iberian margin.

GIs, 8 and 12. Both GIs present significant vegetation, marine and Greenland signals. Figure 6 displays zooms on the intervals 48–40 ka and 40–30 ka encompassing GIs 12 and 8, respectively. According to the evolution of the δD and d excess records, these two GIs have been divided in four subintervals (labeled A–D). Phase A includes the transition in the d excess values between GS and GI, lasting ~100 years, and the maximum values in the δD. Phase B covers the beginning

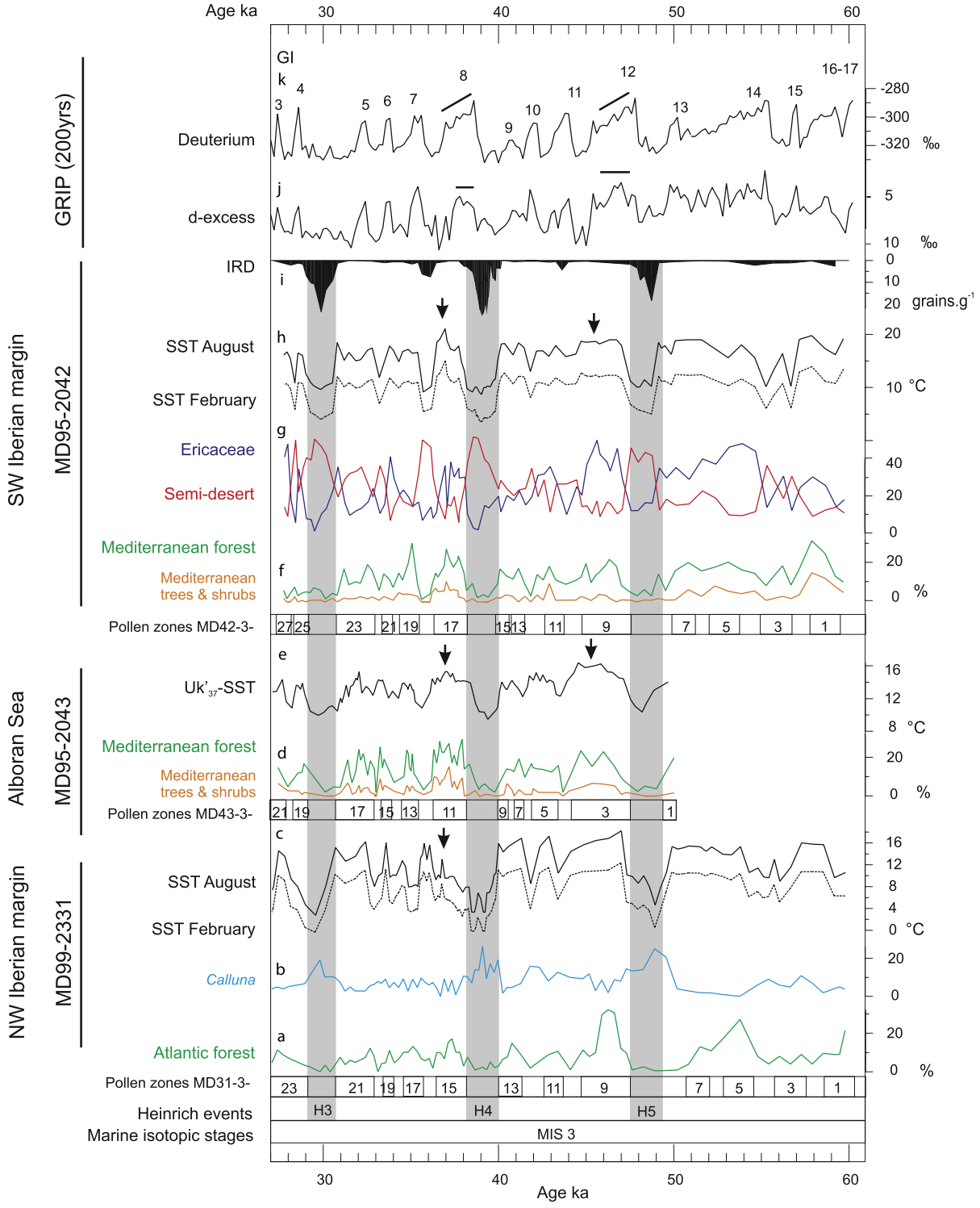

Figure 5

to the middle of the GI: δD decreases slowly thus indicating a decrease of local temperature while d excess is rather stable around its minimum value. Phase C covers the middle to the end of the GI, when δD continues its slow decrease while d excess significantly increases. Phase D covers the transition between the GI and GS and it is marked by a concomitant decrease of δD and increase in d excess within a few centuries.

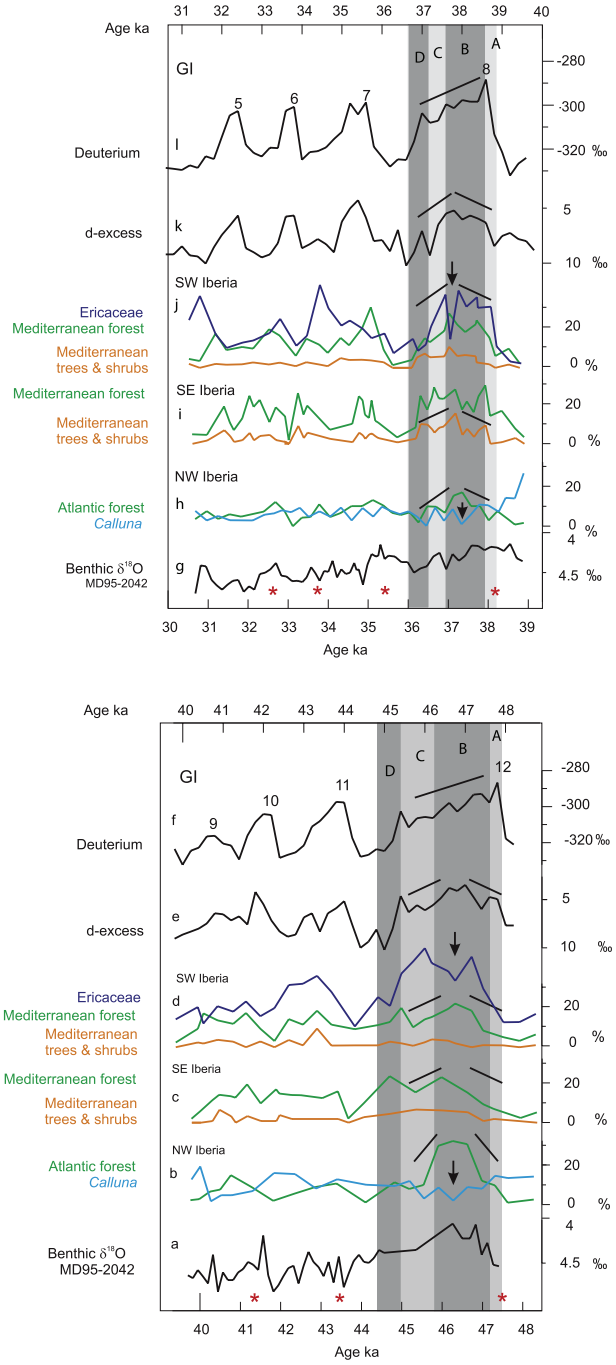

[27] In the Iberian pollen records we can also distinguish the four main phases described above. During phase A all pollen records show a transition from steppe environments (GS) to woodlands (GI) that in some cases occurred extremely rapidly (100–200 years for GI 8 in the Mediterranean region). This interval was also associated with a strong increase in moisture-dependent species (*Calluna* and Ericaceae). Interestingly, none of the pollen records reached the maximum quotes of change during this first phase. During phase B, Mediterranean and Atlantic forests reached their maximum development thus indicating the warmest episode in Iberia during GIs 12 and 8. This phase is also associated with the minimum values of *Calluna* and Ericaceae identifying a concomitant decrease in rainfall in this region. The pollen analysis of core MD95-2039 located in the western Iberian margin at 40°N also shows that the maximum warmth occurred ~1000 years after the onset of GI 12 and 8. The same trend is observed for GI 8 at site ODP 976 in the Alboran Sea, located further west than core MD95-2043. The low resolution of the interval encompassing GI 12 at this site precludes us to detect any particular climate tendency. During phase B, SSTs display, excluding the northern site during GI 12, the highest values at the three sites (arrows in Figure 5), hence indicating the warmest period offshore Iberia. Surprisingly, this observation is not consistent with alkenone-SST reconstructions from site ODP 977 located close to core MD95-2043. This site does not show an increase in SSTs toward the middle of GIs 12 and 8 [*Martrat et al.*, 2004]. In contrast to ODP 977 and supporting the general pattern, alkenone-

Figure 6. Zoom on the interval encompassing GI 8 to 5: (a) Benthic foraminifer δ^{18}O record from core MD95-2042 expressed in VPDB [*Shackleton et al.*, 2000] plotted against the age model used in this study, (b) pollen percentage curves of the Atlantic forest and *Calluna* from core MD99-2331, (c) pollen percentages of Mediterranean trees and shrubs and Mediterranean forest from core MD95-2043, (d) pollen percentages of Mediterranean trees and shrubs Mediterranean forest from core MD95-2042, (e) d excess record from GRIP ice core, and (f) deuterium record from GRIP ice core. Both ice proxies are expressed in V-SMOW. (g–l) Zoom on the interval encompassing GI 12 to 9. The order of the proxy data is the same as in Figures 6a–6f. Grey intervals A, B, C, and D represent the four main phases identified within GI 8 and GI 12. Arrows indicate the low values of moisture-dependent species (Ericaceae and *Calluna*). Red stars indicate the chronological tie points for constructing the age model of the Iberian margin cores.

SST reconstructions from core MD01-2443 [*Martrat et al.*, 2007], a twin core of MD95-2042, shows the highest SST in the middle of GI 8 though GI 12 shows the same trend as the northwestern record (MD99-2331). During phase C a contraction of the Mediterranean and Atlantic forests along with an increase in heathlands occurred indicating cooler and wetter conditions. The transition between GI and GS (phase D) is marked by the collapse of Mediterranean and Atlantic forests being replaced within ~500 years by semidesert and steppe formations in the south and in the north, respectively.

[28] Independently of the timing of the onset of GIs due to the different age models of marine and ice archives, the comparison of the shape of the palaeoclimatic curves from the Iberian margin cores with those from Greenland ice cores permits the description of the mechanism linking the different climatic characteristics of the two regions during major warm phases.

[29] Phase A marked by the sudden increase in Greenland temperature is very probably associated with a strong northward transport of heat stored in the eastern tropical Atlantic Ocean pushing the polar front to high latitudes. In addition to the resumption of the thermohaline circulation (THC) [*Broecker et al.*, 1985], this transport is clearly associated with an atmospheric component as can be seen from the total reorganization of the water cycle depicted by our data: shift from dry to wet conditions in Iberia and northward shift of the moisture source for the Greenland precipitation. Phase B depicts a dissymmetric evolution between low and high latitudes. The slow decrease of temperature in Greenland probably results from the subsequent melting of ice (sea ice or ice sheet) leading to a slow reduction of the heat transport toward high latitudes, probably associated with AMOC (Atlantic Meridional Overturning Circulation) evolution after the strong heat pulse marking the beginning of the GI. This local cooling can also be viewed as a southward shift of the polar front. This cold wave, however, remains confined to relatively high latitudes. Indeed, our data show that the Iberian region has a growing forested cover and increasing temperature over this period. Moreover, the stable d excess indicates that large quantity of moisture can still be exported from relatively high latitudes as in the beginning of the GI implying sufficient heat input. GIs 8 and 12 (phase B) are thus characterized by a stronger climatic gradient between midlatitudes and high latitudes than the beginning of the GI (phase A). This is also nicely seen in our data by the maximum in the forest cover expansion and minimum of Ericaceae percentages revealing temperature increase and precipitation lowering in Iberia in the middle of phase B. This scenario evokes the positive mode of the NAO, i.e., a strong pressure gradient between high and low latitudes directing the westerlies and the associated moisture toward northern latitudes [*Hurrell*, 1995; *Trigo et al.*, 2004]. Such climatic pattern triggers the displacement of the westerlies toward northern Europe favoring the transportation of water from low to high latitudes and thus the observed building of northern ice sheets during GIs [*Rohling et al.*, 2008]. Interestingly the direct correlation between the benthic foraminifer $\delta^{18}O$ curve and the pollen record from core MD95-2042 shows that during GI 8 the forest development in Iberia is concomitant with the increase in $\delta^{18}O$ values though this is less clear during GI 12 (Figure 6). The benthic $\delta^{18}O$ record integrates the signal of global sea level changes, deep water mass temperature and changes in local hydrography. The detailed analysis of the DO variability in deep water properties from a core located close to MD95-2042 shows relatively steady deep warm conditions across the GIs [*Skinner et al.*, 2007]. The benthic $\delta^{18}O$ enrichment along the GIs could reflect a built up of the ice sheet [*Rohling et al.*, 2008] but a substantial part of this signal is associated with major changes in the local deep water hydrography related to AMOC dynamics [*Skinner et al.*, 2007]. Therefore, our own data indicate without any chronological ambiguity, that the warming trend in the Iberian margin and the adjacent landmasses occurred at the same time as changes in AMOC intensity and potentially ice growing in the high latitudes of the Northern Hemisphere.

[30] The third GI phase (phase C) depicts a concomitant decrease in the temperature from Greenland, the Mediterranean and Atlantic Ocean while the T_{source} indicates a warming of the evaporative regions (Figure 2). This can be described as a forward shift of the polar front toward lower latitudes driven by the increase of ice sheets in the high latitudes and slowing down of the AMOC. Because temperature in midlatitudes decreases during this period, the increase of d excess can only be attributed to the southward displacement of the evaporative source regions because of the polar front shift. Note that during this period the climatic gradient between high and low latitudes is reduced thus decreasing the intensity of the ocean-atmosphere transport toward high latitudes. The observed in-

crease of precipitations in Iberia during this phase confirms the reduction of the North Atlantic pressure gradient, similar to the negative mode of the NAO, leading to dryness in northern Europe. Finally, the transition from GI to GS (phase D) is less abrupt than the onset of the DO event (some centuries in Greenland). It follows the slow decrease of the north-south gradient (phase C) and probably indicates a drastic reduction of the ocean-atmosphere transport of heat and humidity toward high latitudes.

6. Conclusion

[31] New high-resolution pollen counting data from the subtropical and midlatitudes of Iberia over MIS 3 allow us to scrutinize the evolution of vegetation and climate in the subtropical/temperate latitudes of the North Atlantic during GIs and to draw a parallel with water isotopic records in central Greenland ice cores. For the two large DO events 8 and 12, our study reveals strong variations in the north-south climatic gradient during the related GIs. After the short-lasting GS-GI transition, Greenland slowly cools down and its precipitation is fed by relatively high latitudes water basins at constant temperature and Iberia experiences a warming and drying episode contemporaneous with apparent changes in the AMOC and ice sheet growth in the high latitudes of the Northern Hemisphere. This scenario suggests the development of a strong pressure gradient during the middle of the GI between high and low latitudes leading to an intense transport of moisture from midlatitudes to high latitudes that can be interpreted as an analog of the present-day positive NAO pattern. Then, the subsequent phase at the end of the GI is a general decrease in high- and low-latitude temperature associated with an increase in Iberian precipitation evoking the climatic patterns associated with the more negative mode of the NAO, hence decreasing the midlatitude to high-latitude moisture transportation and preceding the transition to the GS. Additional high-resolution multiproxy studies in other regions affected at present day by the NAO are needed to constrain the glacial configuration of low- and high-pressure centers in the North Atlantic region.

Acknowledgments

[32] This study was supported by the ESF-EuroCLIMATE RESOLuTION project. We acknowledge the logistic and coring teams on board the R/V *Marion Dufresne II* during IMAGES I and GINNA. We thank S. Desprat and W. Fletcher for their helpful comments on the submitted manuscript. We are grateful to M.-H. Castera, M. Georget, and O. Ther for invaluable technical assistance and V. Hanquiez for the drawing of Figure 1. This is Bordeaux 1 University, UMR-CNRS 5805 EPOC contribution 1732.

References

Birks, H. J. B., and H. H. Birks (1980), *Quaternary Palaeoecology*, 1st ed., 289 pp., Edward Arnold, London.

Blanco Castro, E., et al. (1997), *Los bosques ibéricos*, 1st ed., 572 pp., Planeta, Barcelona, Spain.

Bond, G., W. Broecker, S. Johnsen, J. McManus, L. Labeyrie, J. Jouzel, and G. Bonani (1993), Correlations between climate records from North Atlantic sediments and Greenland ice, *Nature*, *365*, 143–147, doi:10.1038/365143a0.

Broecker, W. S., D. M. Peteet, and D. Rind (1985), Does the ocean-atmosphere system have more than one stable mode of operation?, *Nature*, *315*, 21–25, doi:10.1038/315021a0.

Cacho, I., J. O. Grimalt, C. Pelejero, M. Canals, F. J. Sierro, J. A. Flores, and N. J. Shackleton (1999), Dansgaard-Oeschger and Heinrich event imprints in Alboran Sea paleotemperatures, *Paleoceanography*, *14*, 698–705, doi:10.1029/1999PA900044.

Ciais, P., and J. Jouzel (1994), Deuterium and oxygen 18 in precipitation: Isotopic model, including mixed cloud processes, *J. Geophys. Res.*, *99*, 16,793–16,803, doi:10.1029/94JD00412.

Combourieu Nebout, N., J. L. Turon, R. Zahn, L. Capotondi, L. Londeix, and K. Pahnke (2002), Enhanced aridity and atmospheric high-pressure stability over the western Mediterranean during the North Atlantic cold events of the past 50 k.y., *Geology*, *30*, 863–866, doi:10.1130/0091-7613(2002)030<0863:EAAAHP>2.0.CO;2.

Dansgaard, W. (1964), Stable isotopes in precipitation, *Tellus*, *16*, 436–468.

Dansgaard, W., S. Johnsen, H. B. Clausen, D. Dahl-Jensen, N. Gundestrup, C. U. Hammer, and H. Oeschger (1984), North Atlantic climatic oscillations revealed by deep Greenland ice cores, in *Climate Processes and Climate Sensitivity*, edited by J. E. Hansen and T. Takahashi, pp. 288–298, AGU, Washington, D. C.

Dansgaard, W., et al. (1993), Evidence for general instability of past climate from a 250-kyr ice-core record, *Nature*, *364*, 218–220, doi:10.1038/364218a0.

Fabrès, J., A. Calafat, A. Sánchez-Vidal, M. Canals, and S. Heussner (2002), Composition and spatio-temporal variability of particle fluxes in the Western Alboran Gyre, Mediterranean Sea, *J. Mar. Syst.*, *33–34*, 431–456, doi:10.1016/S0924-7963(02)00070-2.

Fletcher, W. J., and M. F. Sanchez Goñi (2008), Orbital- and sub-orbital scale climate impacts on vegetation of the western Mediterranean basin over the last 48,000 yr, *Quat. Res.*, *70*, 451–464, doi:10.1016/j.yqres.2008.07.002.

Genty, D., D. Blamart, R. Ouahdi, M. Gilmour, A. Baker, J. Jouzel, and S. Van-Exter (2003), Precise dating of Dansgaard–Oeschger climate oscillations in western Europe from stalagmite data, *Nature*, *421*, 833–837, doi:10.1038/nature01391.

Genty, D., et al. (2006), Timing and dynamics of the last deglaciation from European and North African $\delta^{13}C$ stalagmite profiles—Comparison with Chinese and South Hemisphere stalagmites, *Quat. Sci. Rev.*, *25*, 2118–2142, doi:10.1016/j.quascirev.2006.01.030.

Heusser, L. E. (1985), Quaternary palynology of marine sediments in the northeast Pacific, northwest Atlantic, and Gulf

of Mexico, in *Pollen Records of Late Quaternary North American Sediments*, pp. 385–403, Am. Assoc. of Stratigr. Palynol. Found., Dallas, Tex.

Heusser, L. E., and W. L. Balsam (1977), Pollen distribution in the N.E. Pacific Ocean, *Quat. Res.*, *7*, 45–62, doi:10.1016/0033-5894(77)90013-8.

Huber, C., M. Leuenberger, R. Spahni, J. Fluckiger, J. Schwander, T. F. Stocker, S. Johnsen, A. Landais, and J. Jouzel (2006), Isotope calibrated Greenland temperature record over marine isotope stage 3 and its relation to CH_4, *Earth Planet. Sci. Lett.*, *243*, 506–519.

Hurrell, J. W. (1995), Decadal trends in the North Atlantic Oscillation: Regional temperatures and precipitation, *Science*, *269*, 676–679, doi:10.1126/science.269.5224.676.

Johnsen, S. J., W. Dansgaard, and J. W. White (1989), The origin of Arctic precipitation under present and glacial conditions, *Tellus*, *41*, 452–469.

Johnsen, S., D. Dahl-Jensen, N. Gundestrup, J. P. Steffensen, H. B. Clausen, H. Miller, V. Masson-Delmotte, A. E. Sveinbjörnsdottir, and J. W. C. White (2001), Oxygen isotope and palaeotemperature records from six Greenland ice-core stations: Camp Century, Dye-3, GRIP, GISP2, Renland and NorthGRIP, *J. Quat. Sci.*, *16*, 299–307, doi:10.1002/jqs.622.

Jouzel, J. (1999), Calibrating the isotopic paleothermometer, *Science*, *286*, 910–911, doi:10.1126/science.286.5441.910.

Jouzel, J., M. Stiévenard, S. J. Johnsen, A. Landais, V. Masson-Delmotte, A. Sveinbjornsdottir, F. Vimeux, U. von Grafenstein, and J. W. C. White (2007), The GRIP deuterium-excess record, *Quat. Sci. Rev.*, *26*, 1–17, doi:10.1016/j.quascirev.2006.07.015.

Kucera, M., A. Rosell-Melé, R. Schneider, C. Waelbroeck, and M. Weinelt (2005), Multiproxy approach for the reconstruction of the glacial ocean surface (MARGO), *Quat. Sci. Rev.*, *24*, 813–819, doi:10.1016/j.quascirev.2004.07.017.

Landais, A., N. Caillon, J. Jouzel, J. Chappellaz, A. Grachev, C. Goujon, J. M. Barnola, and M. Leuenberger (2004), A method for precise quantification of temperature change and phasing between temperature and methane increases through gas measurements on Dansgaard-Oeschger event 12 (−45kyr), *Earth Planet. Sci. Lett.*, *225*, 221–232, doi:10.1016/j.epsl.2004.06.009.

La Violette, P. E. (1986), Short-term measurements of surface currents associated with the Alboran Sea gyre during Donde va?, *J. Phys. Oceanogr.*, *16*, 262–279, doi:10.1175/1520-0485(1986)016<0262:STMOSC>2.0.CO;2.

Martrat, B., J. Grimalt, C. Lopez-Martinez, I. Cacho, F. J. Sierro, J. A. Flores, R. Zahn, M. Canals, J. H. Curtis, and D. A. Hodell (2004), Abrupt temperature changes in the western Mediterranean over the past 250,000 years, *Science*, *306*, 1762–1765, doi:10.1126/science.1101706.

Martrat, B., J. O. Grimalt, N. J. Shackleton, L. De Abreu, M. A. Hutterli, and T. F. Stocker (2007), Four cycles of recurring deep and surface water destabilizations on the Iberian margin, *Science*, *317*, 502–507, doi:10.1126/science.1139994.

Masson-Delmotte, V., J. Jouzel, A. Landais, M. Stievenard, S. J. Johnsen, J. W. C. White, M. Werner, A. Sveinbjornsdottir, and K. Fuhrer (2005), GRIP deuterium excess reveals rapid and orbital-scale changes in Greenland moisture origin, *Science*, *309*, 118–121, doi:10.1126/science.1108575.

Naughton, F., M. F. Sanchez Goñi, S. Desprat, J.-L. Turon, J. Duprat, B. Malaizé, C. Joli, E. Cortijo, T. Drago, and M. C. Freitas (2007), Present-day and past (last 25000 years) marine pollen signal off western Iberia, *Mar. Micropaleontol.*, *62*, 91–114, doi:10.1016/j.marmicro.2006.07.006.

Ozenda, P. (1982), *Les végétaux dans la biosphère*, 1st ed., 431 pp., Doin, Paris.

Peck, R. M. (1973), Pollen budget studies in a small Yorkshire catchment, in *Quaternary Plant Ecology*, edited by H. J. B. Birks and R. G. West, pp. 43–60, Blackwell Sci., Oxford, U. K.

Pflaumann, U., J. Duprat, C. Pujol, and L. Labeyrie (1996), SIMMAX: A modern analog technique to deduce Atlantic sea surface temperatures from planktonic foraminifera in deep-sea sediments, *Paleoceanography*, *11*, 15–35, doi:10.1029/95PA01743.

Polunin, O., and M. Walters (1985), *A Guide to the Vegetation of Britain and Europe*, 1st ed., 238 pp., Oxford Univ. Press, New York.

Rodwell, M. J., and B. J. Hoskins (2001), Subtropical anticyclones and summer monsoons, *J. Clim.*, *14*, 3192–3211, doi:10.1175/1520-0442(2001)014<3192:SAASM>2.0.CO;2.

Rohling, E. J., K. Grant, C. Hemleben, M. Kucera, A. P. Roberts, I. Schmeltzer, H. Schulz, M. Siccha, M. Siddall, and G. Trommer (2008), New constraints on the timing of sea level fluctuations during early to middle marine isotope stage 3, *Paleoceanography*, *23*, PA3219, doi:10.1029/2008PA001617.

Roucoux, K. H., L. de Abreu, N. J. Shackleton, and P. C. Tzedakis (2005), The response of NW Iberian vegetation to North Atlantic climate oscillations during the last 65 kyr, *Quat. Sci. Rev.*, *24*, 1637–1653, doi:10.1016/j.quascirev.2004.08.022.

Sachs, J. P., and S. J. Lehman (1999), Subtropical north Atlantic temperatures 60,000 to 30,000 years ago, *Science*, *286*, 756–759, doi:10.1126/science.286.5440.756.

Sánchez Goñi, M. F., J.-L. Turon, F. Eynaud, and S. Gendreau (2000), European climatic response to millennial-scale climatic changes in the atmosphere-ocean system during the Last Glacial period, *Quat. Res.*, *54*, 394–403, doi:10.1006/qres.2000.2176.

Sánchez Goñi, M. F., I. Cacho, J.-L. Turon, J. Guiot, F. J. Sierro, J.-P. Peypouquet, J. O. Grimalt, and N. J. Shackleton (2002), Synchroneity between marine and terrestrial responses to millennial scale climatic variability during the last glacial period in the Mediterranean region, *Clim. Dyn.*, *19*, 95–105, doi:10.1007/s00382-001-0212-x.

Sánchez Goñi, M. F., A. Landais, W. J. Fletcher, F. Naughton, S. Desprat, and J. Duprat (2008), Contrasting impacts of Dansgaard-Oeschger events over a western European latitudinal transect modulated by orbital parameters, *Quat. Sci. Rev.*, *27*, 1136–1151, doi:10.1016/j.quascirev.2008.03.003.

Severinghaus, J., A. Grachev, M. Spencer, R. Alley, and E. Brook (2003), Ice core gas thermometry at Dansgaard-Oeschger 8, Greenland, *Geophys. Res. Abstr.*, *5*, 04455.

Shackleton, N. J., M. A. Hall, and E. Vincent (2000), Phase relationships between millennial scale events 64,000–24,000 years ago, *Paleoceanography*, *15*, 565–569, doi:10.1029/2000PA000513.

Skinner, L. C., H. Elderfield, and M. Hall (2007), Phasing of millennial climate events and northeast Atlantic deep-water temperature change since 50 Ka BP, in *Ocean Circulation: Mechanisms and Impacts*, *Geophys. Monogr. Ser.*, vol. 173, edited by A. Schmittner, J. C. H. Chiang, and S. R. Hemming, pp. 197–208, AGU, Washington, D. C.

Stenni, B., V. Masson-Delmotte, S. Johnsen, J. Jouzel, A. Longinelli, E. Monnin, R. Röthlisberger, and E. Selmo (2001), An oceanic cold reversal during the last deglaciation, *Science*, *293*, 2074–2077, doi:10.1126/science.1059702.

Trigo, R. M., D. Pozo-Vazquez, T. Osborn, Y. Castro-Diez, S. Gamiz-Fortis, and M. J. Esteban-Parra (2004), North Atlantic oscillation influence on precipitation, river flow

and water resources in the Iberian Peninsula, *Int. J. Climatol.*, *24*, 925–944, doi:10.1002/joc.1048.

Vautravers, M., N. J. Shackleton, C. Lopez, and J. O. Grimalt (2004), Gulf Stream variability during marine isotope stage 3, *Paleoceanography*, *19*, PA2011, doi:10.1029/2003PA000966.

Vimeux, F., V. Masson, G. Delaygue, J. Jouzel, J. R. Petit, and M. Stievenard (2001), A 420,000 year deuterium excess record from East Antarctica: Information on past changes in the origin of precipitation at Vostok, *J. Geophys. Res.*, *106*, 31,863–31,873, doi:10.1029/2001JD900076.

Voelker, A. H. L., and Workshop Participants (2002), Global distribution of centennial-scale records of centennial-scale records for marine isotope stage (MIS) 3: A database, *Quat. Sci. Rev.*, *21*, 1185–1212, doi:10.1016/S0277-3791(01)00139-1.

von Grafenstein, U., H. Erlenkeuser, A. Brauer, J. Jouzel, and S. J. Johnsen (1999), A mid-European decadal isotope-climate record from 15,500 to 5000 years BP, *Science*, *284*, 1654–1657, doi:10.1126/science.284.5420.1654.

Werner, M., M. Heimann, and G. Hoffmann (2001), Isotopic composition and origin of polar precipitation in present and glacial climate simulations, *Tellus, Ser. B*, *53*, 53–71.